Published by Associazione Teriologica Italiana
Hystrix, the Italian Journal of Mammalogy
Volume 30 (2): 157–165, 2019
OPEN ACCESS
Available online at:
http://www.italian-journal-of-mammalogy.it
doi:10.4404/hystrix-00206-2019

Research Article

Seeing the wood through the trees. Combining shape information from different landmark configurations

Antonio Profico[1,2,*], Paolo Piras[1], Costantino Buzi[1], Antonietta Del Bove[4,5], Marina Melchionna[6], Gabriele Senczuk[7], Valerio Varano[8], Alessio Veneziano[9], Pasquale Raia[6], Giorgio Manzi[7]

[1]*Dipartimento di Biologia Ambientale, Sapienza Università di Roma, Rome (Italy)*
[2]*PalaeoHub, Department of Archaeology, University of York, York (United Kingdom)*
[3]*Dipartimento di Scienze Cardiovascolari, Respiratorie, Nefrologiche, Anestesiologiche e Geriatriche, Sapienza Università di Roma, Rome (Italy)*
[4]*Catalan Institute of Human Paleoecology and Social Evolution (IPHES), Tarragona (Spain)*
[5]*Àrea de Prehistòria, Facultat de Lletres, Universitat Rovira i Virgili, Tarragona (Spain)*
[6]*Dipartimento di Scienze della Terra, dell'Ambiente e delle Risorse, Università di Napoli, Federico II, Naples (Italy)*
[7]*Dipartimento di Biologia e di Biotecnologia, Sapienza Università di Roma, Rome (Italy)*
[8]*Dipartimento di Architettura, Università degli Studi di Roma Tre, Rome (Italy)*
[9]*Sincrotrone Trieste, SYRMEP, Trieste (Italy)*

Keywords:
geometric morphometrics
morphology
skull
primates
2D images
combinland

Article history:
Received: 29 May 2019
Accepted: 10 September 2019

Acknowledgements
We thank two anonymous reviewers for their help in improving the quality of the manuscript. We also thank Andrea Cardini for useful suggestions and insights.

Abstract

The geometric morphometric (GM) analysis of complex anatomical structures is an ever more powerful tool to study biological variability, adaptation and evolution. Here, we propose a new method (*combinland*), developed in R, meant to combine the morphological information contained in different landmark coordinate sets into a single dataset, under a GM context. *combinland* builds a common ordination space taking into account the entire shape information encoded in the starting configurations. We applied combinland to a Primate case study including 133 skulls belonging to 14 species. On each specimen, we simulated photo acquisitions converting the 3D landmark sets into six 2D configurations along standard anatomical views. The application of *combinland* shows statistically negligible differences in the ordination space compared to that of the original 3D objects, in contrast to a previous method meant to address the same issue. Hence, we argue *combinland* allows to correctly retrieve 3D-quality statistical information from 2D landmark configurations. This makes *combinland* a viable alternative when the extraction of 3D models is not possible, recommended, or too expensive, and to make full use of disparate sources (and views) of morphological information regarding the same specimens. The code and examples for the application of *combinland* are available in the `Arothron` R package.

Introduction

Ever since Blumenbach et al. (1865) the study of cranial morphology makes use of linear measurements allowing to compare individuals and species. The later development of geometric morphometrics (GM) paved the way for the study of morphological variation avoiding to reduce "shape" down to a set of linear measurements (or ratios) of some sort (Rohlf, 2000). GM is much more accurate of linear measurements as a shape descriptor. Consequently, GM represents the most common method to quantify size and shape variations in biological and paleobiological applications (Rohlf and Marcus, 1993; Jungers et al., 1995; Adams and Rohlf, 2004; Adams et al., 2013; Piras et al., 2009, 2010, 2014; Sansalone et al., 2015; Neaux et al., 2018).

Under GM, either two- (2D) or three-dimensional (3D) configurations of landmarks are recorded. The former (2D) approach relies on the pictorial representation of the biological objects of interest (e.g. pictures, X-ray, MRI) (Bastir and Rosas, 2009, 2006; Adams and Rohlf, 2004; DeQuardo et al., 1999), whereas the latter works by recording the landmarks directly on the three-dimensional object, as represented by either the real item of interest (i.e. using 3D digitizers) or by digital reconstructions acquired through computer tomography, laser scanning, or photogrammetry (Profico et al., 2018a; Olsen and Westneat, 2015; Weber, 2015; Bates et al., 2010). One major advantage of 2D over 3D data is that they are more easily acquired visiting museum collections or any other repository and a wealth of 2D data (pictures) are readily available online through published sources. The acquisition of 2D data is fast and relatively inexpensive, so that sample size almost always rises above those typical for 3D studies. During the last decades the increased availability of 3D digital repositories is spurring interest on 3D geometric morphometrics (Cardini, 2014; Davies et al., 2017). This is welcome since the morphological information that comes with 3D objects is richer and more genuine than with 2D samples, which suffers from shape distortion due the "parallax problem" (Mullin and Taylor, 2002), and are further limited to a single view of the objects of interest (Ponton, 2006). Unfortunately, the acquisition of 3D data is still expensive and time-consuming (Cunningham et al., 2014). Moreover, 3D models often require post-production to refine the quality of the digital specimens (e.g. decimation and smoothing procedures, Veneziano et al., 2018) which further lengthens the data processing time.

In this study, we propose a new statistical approach which combines multiple 2D datasets into a unique matrix that can be subjected to ordination analyses encoding the whole morphological information. The most straightforward way to test this tool is the recovery of 3D morphological information starting from different 2D views. It must be emphasized, though, that our approach can be used to combine different 2D or 3D configurations or even 2D and 3D configurations together. It is similarly important to remark that our purpose is not to build the 3D geometry via single 2D views, as done by photogrammetry. Instead,

*Corresponding author
Email address: antonio.profico@uniroma1.it (Antonio Profico)

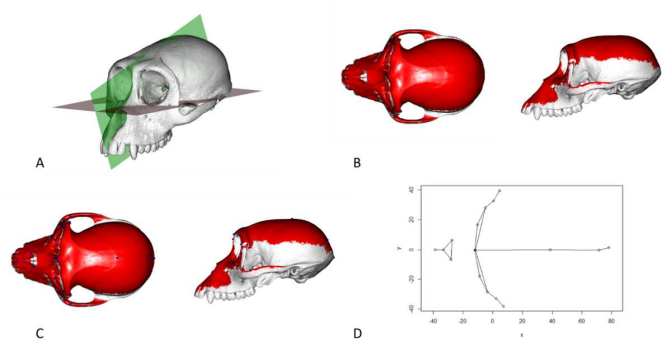

Figure 1 – Protocol used to convert a 3D landmark configuration into six different 2D sets. The midsagittal (in green) and Frankfurt (in red) planes are reported on a *Macaca arctoides* 3D model (A). The visible triangles (B) of the mesh and the visible landmarks (C) from the point of view set on superior view are reported in red and blue respectively. 2D landmark set with wireframe of a specimen of *Macaca arctoides* in superior view (D).

we want to build a common ordination space starting from shapes acquired with different number of landmarks in both 2D or 3D.

The method ("*combinland*"), is based on a technique originally proposed by Adams (1999). *combinland* works by merging the morphological information obtained from the Generalized Procrustes Analysis (GPA) of different datasets into a single matrix of coordinates. Differently from the traditional method (Adams, 1999; Davis et al., 2016; Meloro et al., 2017), in *combinland* we introduced a new size correction to guarantee a proper combination of multiple landmark configurations weighting sizes for the number of landmarks and dimensions. In addition, in *combinland* we supply a solution to calculate and plot the shape variations of each combined landmark configuration associated to the extreme values of the PC scores, in keeping with the issue of improving the visualization of shape changes in GM applications (Klingenberg, 2013). We assessed the performance of *combinland* using a 3D dataset from which we derived six 2D datasets (referring to specific anatomical views) to assess whether the combined 2D information compares well to 3D data, considered as "ground truth". We provide the R code, embedded in the `Arothron` R package (Profico et al., 2019), to apply *combinland* to 2D datasets.

Materials and methods

3D and 2D datasets: the Primate case study

We sampled, in 3D, 55 landmarks (Fig. S1) over the cranial surfaces of 14 Primate species belonging to Catarrhini (10 species) and Platyrrhini (4 species) for a total of 133 specimens (see Tab. S2 for details). Starting from the 3D objects, we produced six 2D datasets for each specimen, defined along the six main anatomical views (i.e., frontal, superior, inferior, posterior, right lateral and left lateral) used in anthropology, which refer to the midsagittal and the Frankfurt planes, respectively. The midsagittal plane is defined by the *prosthion*, *bregma* and *basion* anatomical points. The Frankfurt plane is defined by different points (here digitized as landmarks): the left *orbital* (intended as the lowest point on the orbital rim) and both left and right *poria*. The left- and the right-lateral 2D sets (1–2) are defined by projecting the 3D coordinates orthogonally onto the midsagittal plane, the superior and the inferior sets (3–4) are obtained projecting the 3D set onto the Frankfurt plane. Finally, the posterior and the anterior sets (5–6) are calculated in two steps: i) the rotation of the Frankfurt plane of $\pi/2$ radians and ii) projection of the 3D coordinates on the plane.

By using 3D digital models, visible landmarks can be defined with respect to a point of view (POV) external to the object. Straight lines are projected from the POV coordinates towards each landmark. If the projection line intersects the 3D object external surface before reaching the landmark, the latter is defined as non-visible, or visible otherwise. The method, referred to as CA-LSE (Computer Assisted Laser Scanner Emulator) is described in Profico and colleagues (2018b; see Fig. 1).

After defining 2D landmarks configurations, we performed a Generalized Procrustes Analysis (GPA), without scaling, on each 2D set. The third dimension was intentionally set to zero in such configurations, as it happens when taking digital pictures of the specimens. The procedure is summarized in Fig. 1. We obtained six 2D datasets of landmark in left-lateral (N=24), right-lateral (N=24), superior (N=17), inferior (N=40), posterior (N=16) and anterior (N=20) anatomical views (see Fig. S3 and Tab. S4). It is crucial to note here that our conversion from 3D into six 2D configurations does not realistically mimic the 2D photo acquisition of an osteological collection from the different anatomical views. Our procedure does not simulate the potential effect of Parallax problem due to the distortion or lens positioning intrinsically present in photographs (see Discussion section).

The "*combinland*" method

Under "*combinland*" separate GPAs are performed for each 2D anatomical view, separately, and scaled to the unit Centroid Size (*CS*). In geometric terms the *CS* represents the quadratic mean of the projections, along each of the *m* coordinate directions, of the vector difference between each landmark and the centroid. At this stage, the 2D datasets are not comparable. In fact, *CS* cannot be used to compare sizes of shapes identified by different number of landmarks. A convenient way to normalize the *CS* (size correction) is to divide it by the square root of the number of landmarks times the number of dimensions (as suggested in Dryden and Mardia, 2016, section 2.2.2). This quantity gives the quadratic mean squared distance of the landmarks to their centroid, i.e. the $k \times m$ components (where k is the number of landmarks and m is that of dimensions) of the centred configuration matrix. The six corrected (by the number of landmarks) matrices of aligned coordinates are appended together to compose a single matrix (2DComp), which is then subjected to principal component analysis (PCA). The PC scores extracted from 2Dcomp represent the descriptors of the whole morphological variation encoded in the combined 2D data. The procedure is summarized in Fig. 2.

In sum, the protocol applied herein consists of 5 steps: i) capturing the 2D landmark configurations according to the six standard anatomical views, ii) performing a GPA on each of the six 2D datasets, iii) applying "size correction" to the six sets of aligned coordinates derived from GPA: this size correction consists in re-multiplying coordinates (that were originally divided by their proper *CS*) by the square root of their number of landmarks (that vary among different configurations) times their number of dimensions (that in this specific case is always 2, see below), iv) appending the six matrices of corrected coordinates, v) performing PCA on the new data matrix. Points ii to v represent *combinland*.

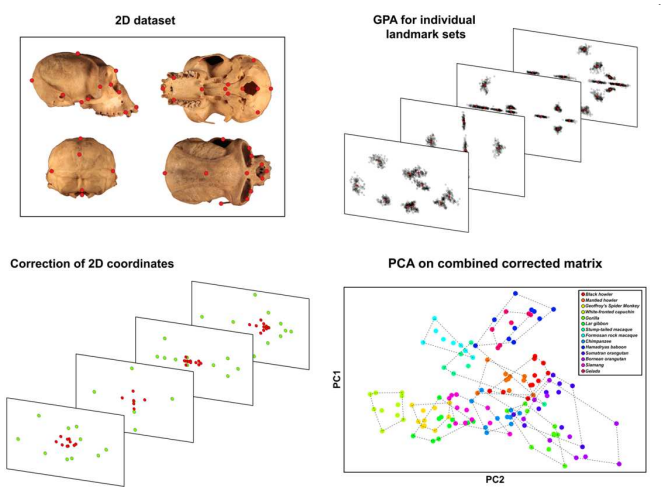

Figure 2 – The "*combinland*" method. Landmarks are recorded separately on different anatomical views (A). GPA is performed on each 2D datasets (B). The 2D sets after GPA are corrected by the square root of the number of landmarks times the number of dimensions of each set (red and green: before and after correction, respectively) (C). Merging of the corrected coordinates (2D datasets) and PCA on the new matrix of coordinates (D).

To visualize the shape variations for each of the six 2D views associated to the combined data we used: i) the mean shapes corresponding to 2D datasets of the coordinates after GPA. The coordinates of these mean shapes are re-multiplied by the square root of the number of landmarks of the corresponding 2D view times the number of dimensions. ii) the sub-matrix corresponding to those landmarks belonging to a particular 2D view from the eigenvalue matrix coming from the PCA performed on the combined (size-corrected) 2D coordinates corresponding only to the 2D landmarks set that is needed for visualization. iii) the values of the PC scores for which the visualization is called.

We also compared the shape variations predicted by 3D PCA with those coming from *combinland* PCA projecting the PCA-predicted 3D shapes on the same planes used to obtain 2D landmark sets. To assess the differences between the shape variations coming from 3D data and those from 2D combined data we calculated the Procrustes Distances between the projections of shapes predicted by PCA on true 3D data and those coming from PCA on combined 2D data.

Geometric morphometrics, centroid size and biological implications

Size variability affects shape variation in biological structures. Under GM shape is defined as "the geometric information that remains when location, scale and rotational effects are filtered out from an object" (Kendall, 1977). In turn, such geometric information is defined by the acquisition of the coordinates of landmarks corresponding to homologous anatomical points. The Generalized Procrustes Analysis (Gower, 1975) removes the information of the components of location, scaling and rotational. The size component is habitually defined as the square root of sum of the squared distances between landmarks and the centroid of the configuration (Bookstein, 1989). According to Bookstein (1986) *CS* is therefore uncorrelated with shape under the assumption that the variation around each landmark mean is represented by small, independent, identically distributed circular normal errors. However, this assumption cannot account for the true error distributions and thus there is no inherently best size measure. In continuum mechanics, for example, the m-Volume is the most used size measure (Varano et al., 2018) as it is specifically related to a physical domain of the body under study (m-Volume has a unit of measurement, *CS* does not), a concept that could become very elusive when dealing with single digitization of points sparse in complex structures. The mathematic formulation of *CS* pretends it is correlated to the "actual size" of the anatomical traits. However, any size measure should reflect the true physical size of the object under study. It follows that identical structures, digitized in different ways, should have or identical or approximately equal sizes. Nevertheless, the value of *CS* is influenced by the total number of landmarks defining the shape and the contribute made by each landmark is proportional to its squared distance to the centroid (Fig. 3).

As it stands, the *CS* increases with increasing number of landmarks and is influenced by the squared distance of landmarks to the centroid. Under conventional GM studies this is not relevant, because the same configuration applies to all specimens. Yet, it becomes relevant when combining different configurations. To fix this problem, we propose a different solution from Adams (1999) and Davis et al. (2016), by computing the relative size of different norms in reference to the total dimension of the considered norms. In particular, Adams (1999) and Davis et al. (2016) combine two different views (F and S) each with their proper size CS^F and CS^S of a digitized structure into a single dataset that parameterizes the single sizes on their sum (Eq. 1):

$$\begin{aligned} CS^F &= \frac{CS_F}{CS_F + CS_S}, \\ CS^S &= \frac{CS_S}{CS_F + CS_S}, \end{aligned} \tag{1}$$

where superscript ^{F} and ^{S} correspond respectively to the F and S relative components of the centroid size (CS).

Defining each anatomical view as $k \times m$, where k is the number of landmarks and m is the number of dimensions (2D or 3D) we divided the CS by $\sqrt{km}$ (as proposed in Dryden and Mardia, 2016, section 2.2.2):

$$\begin{aligned} CS^F &= \frac{CS_F}{\sqrt{k_F m_F}}, \\ CS^S &= \frac{CS_S}{\sqrt{k_S m_S}}. \end{aligned} \tag{2}$$

A simple simulation proves this point. We digitized two circle outlines placing 10 and then 100 landmarks, respectively (Fig. 4 a,b). From each configuration, we generated 300 landmark-wide configurations using the Dryden and Mardia (2016) model (Fig. 4) and calculated the mean relative sizes of each configuration using either our *CS* correction (Eq. 2) or using `combine.subsets` (Eq. 1) function in `geomorph` package (Adams and Otárola-Castillo, 2013) which is based on the approach of Davis et al. (2016).

By using our method, the relative *CS* for the two datasets are both equal to 0.50. The mean values of the relative *CS* after the application of Equation 2 (Davis et al., 2016) are equal to 0.24 and 0.76 respectively.

A simulated example

A simulated example shows the efficacy of *combinland CS* correction. We started by producing two 2D configurations with a different number of landmarks. The first dataset is defined starting from an "irregular polygon shape" configuration, the second one from a "circular shape" configuration. On these shapes we applied non-affine deformation cycles (Piras et al., 2016). The cycles apply a combination of aspect ratio and bending. This way, we produced 2D datasets of shapes each with 10 and 200 landmarks from the "irregular" and "circular" shapes respectively. Successively, we converted the 2D shapes into 3D

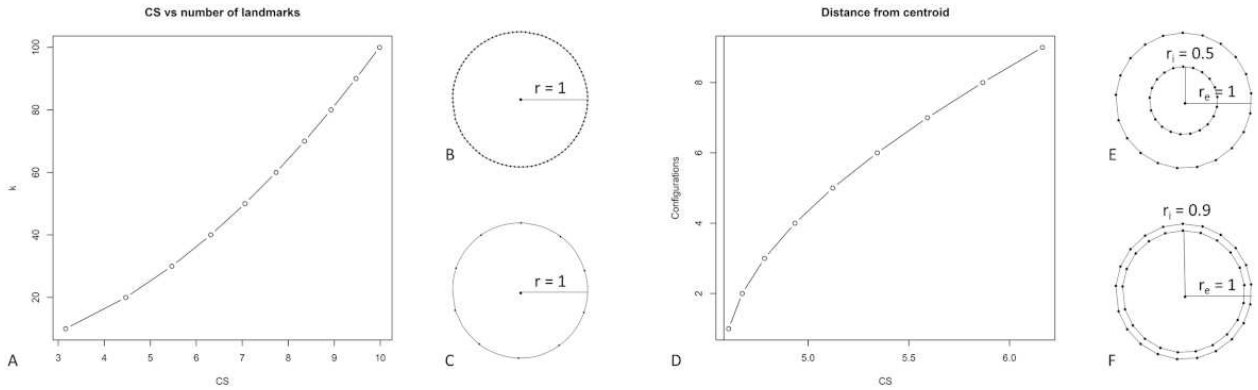

Figure 3 – Biplots showing the relation between Centroid Size (*CS*) and number of landmarks (*k*) (A). In this example, the structure (a single circle of radius=1) is the same in all of the 10 configurations (where B and C are two examples). On the right the relation between Centroid Size (*CS*) and distance from centroid (*D*) is shown. In this example, the structures (two concentric circles) has been digitized using the same number of landmarks (for a total of 42): the external circles have the same radius (r=1) in all the configurations while the internal ones are progressively scaled (e.g. E and F, the range of the radii for the internal circles, *ri*, is bracketed between 0.1 and 0.9). The vertical line shows the *CS* values of the structure without the inner circle.

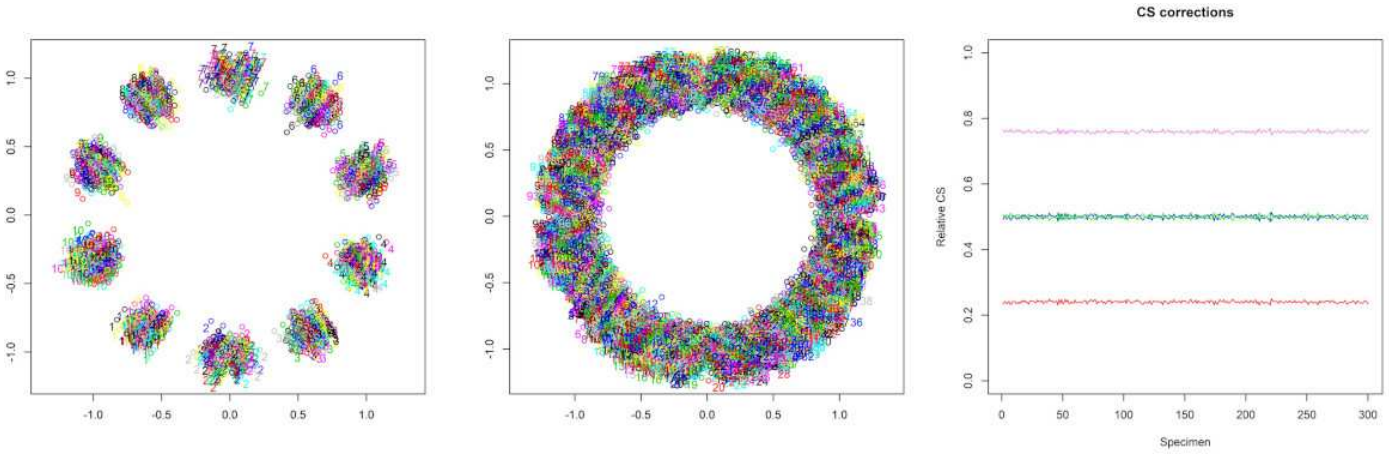

Figure 4 – Experiment: simulated datasets (for a total of 300 specimens) consisting of two hypothetical anatomical views that possess exactly the same circular shape. The first one (F) is defined by 10 landmarks, the second one (S) is defined digitizing 100 landmarks. On the right the two *CS* corrections are reported. The relative *CS* after the correction published by Davis and colleagues (2016) is shown as red (F view) and violet (S view) lines. The relative *CS* after the application of the correction proposed in this work is reported in blue (F view) and green (S view).

landmark configurations adding a third dimension each, perpendicularly to the *x*-*y* and *x*-*z* planes respectively, for the two configurations, centered at the origin (Fig. 5).

From the 2D datasets, we thus have i) a combined version with the size correction (*combinland*), ii) a combined version without size correction iii) a 3D dataset. For each of the three datasets we performed a PCA after Procrustes registration. In Fig. 6 we reported the three resulting PCA plots.

In order to compare the PCA spaces we adopted the same strategy used in Varano et al. (2017): we calculated the Riemannian distance between the shapes identified by the scores of the first two PC scores (Fig. 6). These shapes are approximately elliptical. In each of the three analyses the first two PC scores summarize approximately 97% of total variance. The Riemannian distances between the shapes identified by the first two PC scores of the 3D dataset and those identified by the first two PC scores of the combined 2D datasets using *combinland* is 0.008. This same distance rises to 0.060 without correction. Eventually, we calculated the geodesic distance of the UPGMA cluster built using the first two PC scores coming from 3D dataset with those coming from the two combined 2D datasets (see Fig. S5), i.e. with and without size correction; they are equal to 0.27 and 5.87 respectively. Figure 7 shows the shapes predicted at max and min values of PC1 and PC2 for the two substructures as predicted by combining the data with size correction, without size correction and on 3D data, respectively, showing how close the size-corrected data come to 3D. A Mantel test performed between the PC scores coming from the 3D dataset and those of PCA that uses *combinland* is equal to 1. The same test performed between the 3D dataset and the PC scores from combined 2D data without applying the size correction returns a value equal to 0.95. Although apparently minimal, this result confirms the appropriatedness of the size correction procedure.

This result is further confirmed by the calculation the Procrustes distances between the shape variations from 3D data and those calculated from the 2D data with and without the size correction (Tab. 1). The difference between the shape variations from 3D and combined 2D data with size correction calculated at the extremes of the first two PC scores are negligible (Tab. 1).

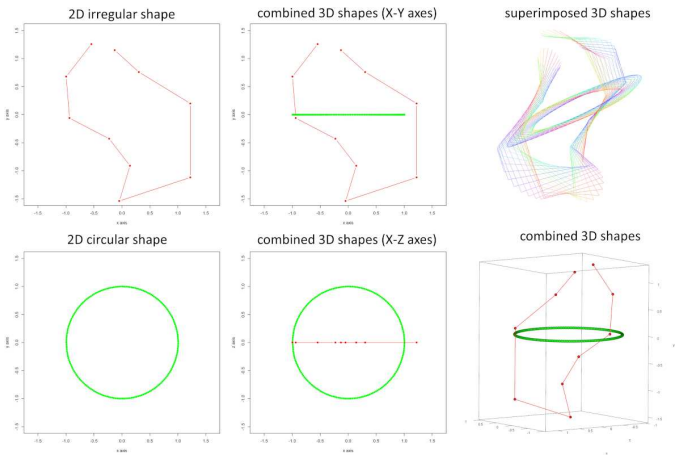

Figure 5 – Plot of the first undeformed specimen belonging to the simulated case study. On the left column the two 2D-landmark configurations (irregular and circular shapes); these configurations refer to shapes that possess approximately the same physical size. In the middle the combined 3D landmark configuration shown on XY and XZ axes. At top right the full combined 3D dataset consisting on the deformation of the first shape after Procrustes registration. The 3D landmark configuration is also shown (bottom right).

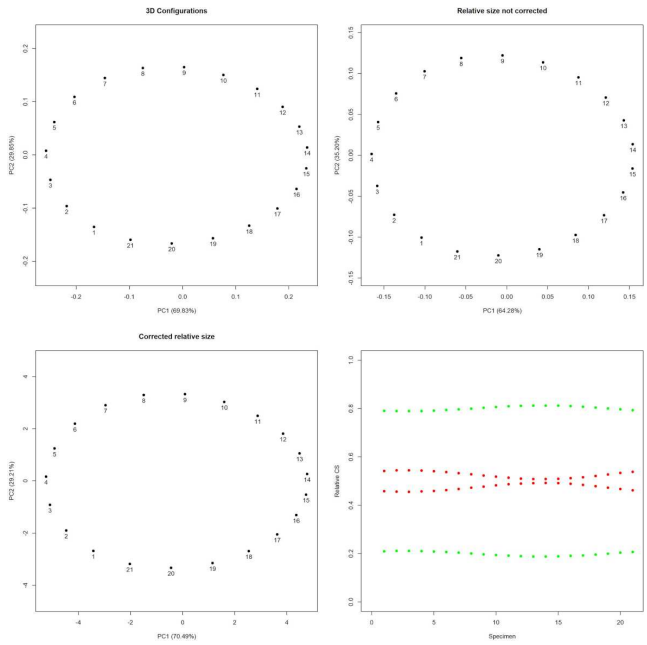

Figure 6 – PCA plots performed on the 3D original landmark configuration (top left) and on the 2D combined landmark configurations without (top right) and with (bottom left) size correction. At bottom right, the relative sizes of the two 2D combined datasets compared to the entire configuration resulting by merging them in a single shape. Only the size-corrected configurations (red dots) appear insensitive to the number of landmarks per configuration thus returning similar CS values. The same does not apply for non-corrected configurations (green dots) that give green values approximately four times greater than the red ones.

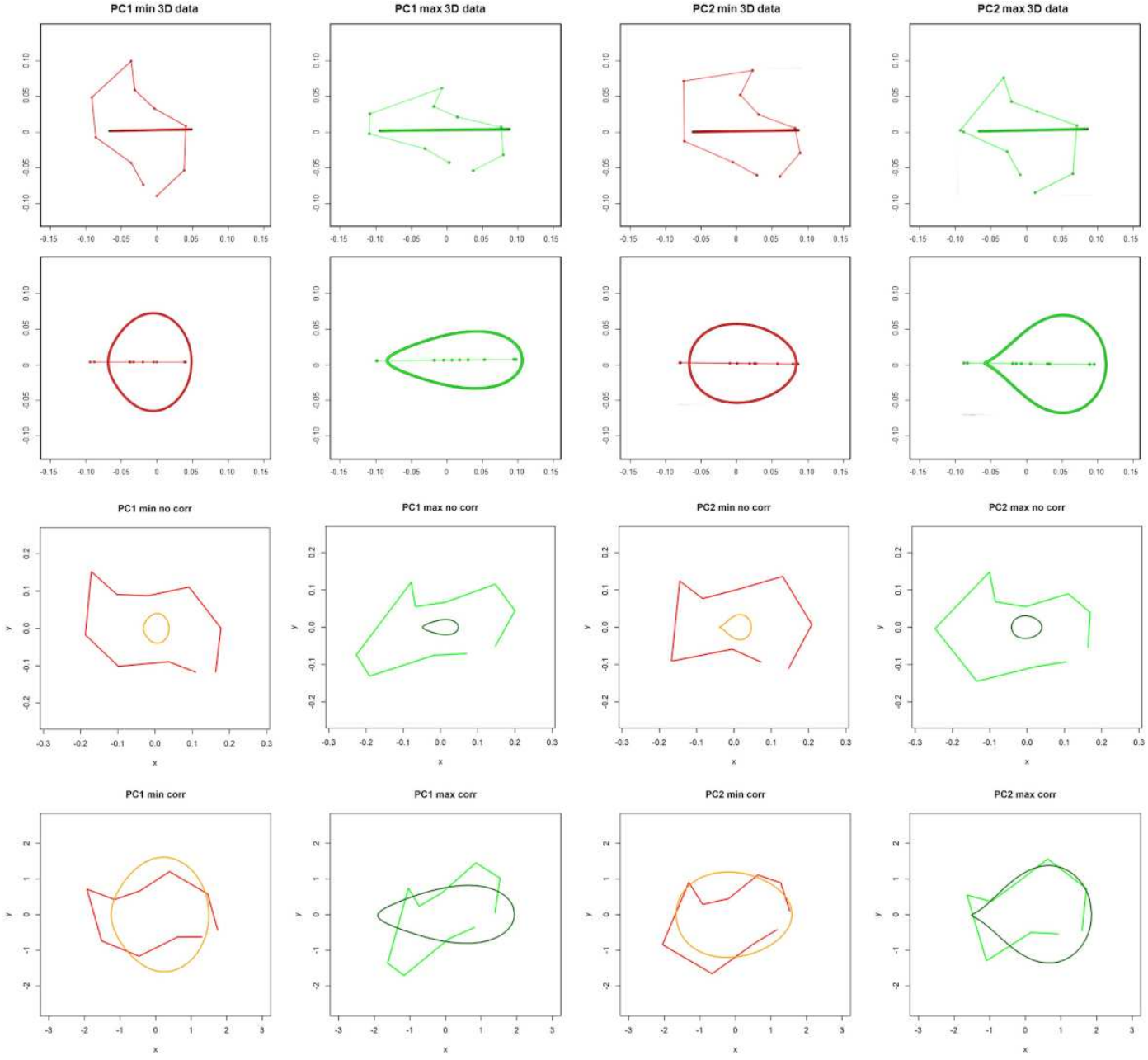

Figure 7 – Shape variations associated at the extremes of the first two principal components for 3D and 2D combined datasets (with and without size correction). To save space we reported in the same panel the two shape variations of 2D combined data predicted by PC extreme values associated to the irregular and circular shapes. The first two rows show the shape variations of 3D data, i.e. the irregular and circular shapes, the third row the shape variations corresponding to the combined 2D data without size correction (circular and irregular shapes on the same panel), the fourth row the shape variation of the combined 2D data with size correction (circular and irregular shapes on the same panel). It can be seen that a drastic size bias is present in the third row.

Table 1 – Procrustes distances calculated between 2D projections of shapes predicted at extremes of the first two PC scores of 3D data and corresponding 2D shapes predicted by the PCA performed on the combined 2D dataset with (our method) and without size correction. We reported the values for the two shapes ("Irregular" and "Circular").

PC score	Shape	No size correction	With size correction
PC1 min	Irregular	0.0105	0.0108
	Circular	0.0630	0.0010
PC1 max	Irregular	0.0111	0.0090
	Circular	0.0087	0.0007
PC2 min	Irregular	0.3718	0.0114
	Circular	0.1347	0.0001
PC2 max	Irregular	0.3747	0.0103
	Circular	0.1346	0.0007

Evaluation of *combinland* performance on Primate skulls

To assess the performance of *combinland* in the real Primate skull case, we compared the PCA coming from the 3D data (3D data) with the PCA on the 2D data processed under *combinland* and under the strategy without size correction.

The PC scores of the entire shape of all datasets (3D and 2D) were subjected to cluster analysis using the Unweighted Pair Group Method with Arithmetic mean (UPGMA, Sokal and Michener, 1958). We defined and combined two categorical variables for each specimen: species and gender. By using UPGMA trees, we checked how well the 2D data reproduces the 3D trees topology. The use of phenetic trees to assess *combinland* performance is crucial because the error introduced using 2D data to represent 3D objects can be as large as the shape distance between two species (Cardini, 2014). The similarity between 2D and 3D clusters was quantified by using both the geodesic and the edge set distances. The geodesic distance is the sum of the difference between the corresponding path between two weighted phylogenetic trees. The edge set distance is computed as sum of the differences between the number of internal branches and/or inversions between two weighted phylogenetic trees (Chakerian and Holmes, 2012; Owen and Provan, 2011).

We scaled the edge length of the trees by imposing an equal (arbitrarily unitary) total edge length. The six anatomical views can be combined into smaller subgroups of size n (where n represents the number of 2D views combined together). For k=6 anatomical views there are $2k - 1 = 63$ possible combinations of 2D sets (from the six each with only one configuration to the one including all of them). We produced 63 UPGMA-based cluster analyses, one for each of the 63 possible combinations. Subsequently, we calculated for each of the 63 UPGMA trees the geodesic and the edge set distance from the UPGMA tree built using the PC scores of the 3D data. Eventually, we evaluated the covariation between the PC scores coming from the 3D and 2D data (with and without landmark's number correction) by Partial Least Squares (PLS) analysis (Rohlf and Corti, 2000).

In addition, we performed the Mantel test between the matrix of PC scores of the 3D data and the PC scores of the combined 2D data (with and without the "size correction") appending the two, three, four, five and six anatomical views generating all the 57 possible combinations.

We further evaluated *combinland* performance by comparing the shape variation explained by 3D PCA with those explained by the combined 2D sets. In detail, we produced six bi-dimensional projections of 3D shape variations predicted at positive and negative extreme values of the PC scores, applying the same projection protocol used to create the 2D datasets.

We also compared the eigenvectors coming from separate PCA performed on these two arrays: the first one is related to the shape variations associated to the extreme values (minimum and maximum) of the first three PC scores of the 2D data; the second one refers to the shape variations of the 3D dataset projected into two-dimensional Cartesian system. This analysis aims at verifying whether, besides correlation between scores, the morphologies explained by the ordination methods are actually similar. In addition, we combined these two types of arrays into one and we performed a PCA. 3D and 2D shapes corresponding to the same PC extremes should result in "coupled" data. We also performed an analysis of evolutionary allometry in Platyrrini, Cercopithecoidea, Hominoidea evaluating the effect of the same size regressor (CS from 3D data) on the shape from 3D and 2D datasets (with and without "size correction").

Eventually, we compared the shapes of each specimen from the 3D PCA with those obtained from the combined 2D analyses. The two datasets consist on the shapes identified by the first 20 PCs in the PC space of the corresponding analyses (explaining collectively more than 95% of total variance). From the 3D PCA, we calculated for each specimen six bi-dimensional shapes using the six anatomical views used in the combined 2D analyses. To quantify the differences between them, we calculated the partial Procrustes distance normalized on the maximum distance allowed (that is $\sqrt{2}$, Varano et al., 2017).

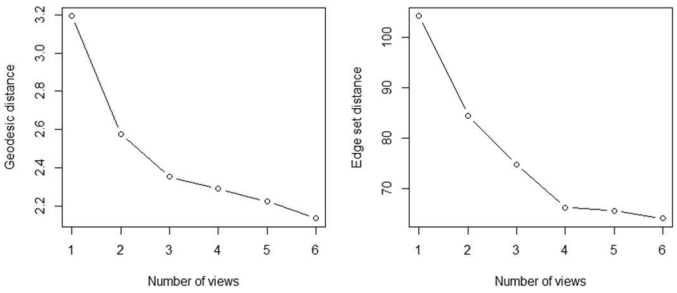

Figure 8 – Cumulative variance explained by the first 5 PCs in the 3D (left) and combined 2D (right) data. The percentage of variance explained by each of the first 5 PCs is reported in the plot.

Results

Principal Component Analysis on 3D and 2D data

The first two PC scores of the 3D and 2DComp data explain together the 53.21% and the 51.45%, respectively, of the total variance (Fig. 8). In the two plots (3D and 2D) the Cercopithecoidea (*Macaca*, *Papio* and *Theropithecus*) are located on the positive value of the PC1 close to the great Apes (*Pan*, *Gorilla* and *Pongo*). New World monkeys (*Cebus*, *Ateles* and *Alouatta*) and hylobatids (*Hylobates* and *Symphalangus*) occur at the negative values of the PC1. Along PC2 there is a clear distinction between the group formed by *Pongo* and *Alouatta* from all other species (Fig. 9).

The morphological variation associated to the first two PCs of 3D and combined 2D analyses are very similar (Fig. 10). From the anterior view, the pattern of shape variation along the PC1 is associated with the maximum height of the face and the relative shape and position of the piriform aperture: along positive values the face and the nasal aperture are high. PC2 is mainly associated to facial width: at positive values the facial complex broadens (Fig. 10). From the posterior view, PC1 captures variation associated to the position of the *poria*. PC2 records

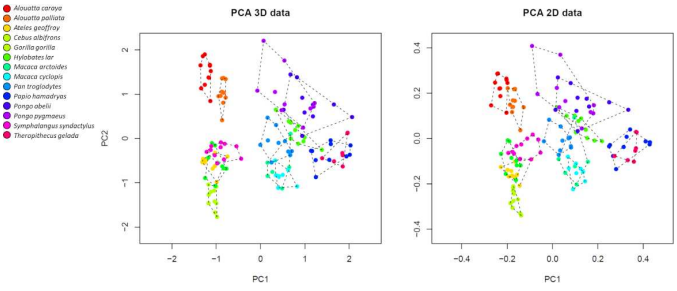

Figure 9 – Plot of the first two PCs of the 3D (left) and combined 2D Primate data (right). A convex hull encloses each species: *Alouatta caraya* in red, *Alouatta palliata* in orange, *Ateles geoffrey* in gold, *Cebus albifrons* in yellow green, *Gorilla gorilla* in green, *Hylobates lar* in dark green, *Macaca arctoides* in light blue, *Macaca cyclopis* in cyan, *Pan troglodytes* in light sky blue, *Papio hamadryas* in blue, *Pongo abelii* in slate blue, *Pongo pygmaeus* in violet, *Symphalangus syndactylus* in fuchsia and *Theropithecus gelada* in magenta.

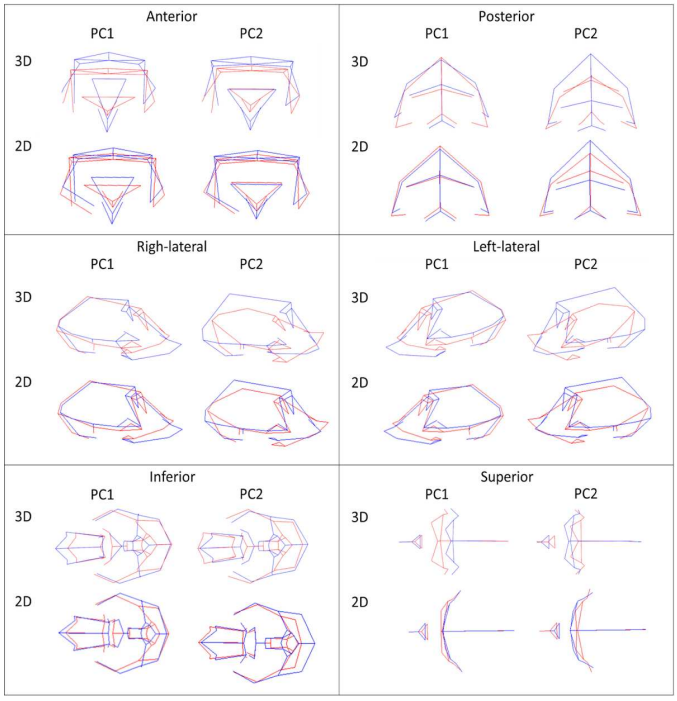

Figure 10 – Shape variations associated to negative (red) and positive (blue) extreme values of the first two principal components for the 3D and combined 2D data.

the relative positions of *bregma* and *asteria*. Still, a change associated to the orientation of the *foramen magnum* seems discriminating among specimens (Fig. 10). In lateral view, PC1 captures the rate of the alveolar prognathism. Along PC2, shape changes associate to the degree of airorhynchy (Fig. 10).

From the superior view the most prominent shape changes relate to the lengthening of the skull (PC1) and to the relative position of the supraorbital region (PC2). At positive values of PC1 the supraorbital region appears shifted posteriorly (Fig. 10).

Along PC1, from the inferior view, shape change associated to the anterior shifting of the *foramen magnum* is well distinct at positive values of this vector. PC2 records the relative size of the occipital bone, that is broader at positive values. Also, the relative size of the *foramen magnum* is affected: at positive values it appears broader than at negative values (Fig. 10). These results indicate that *combinland* provides realistic shape variation information as compared with the 3D data, at least when 6 different views are combined together.

Performance of the combinland method

The geodesic and edge set distances calculated on the UPGMA trees (Fig. S6–S8) produced by using the PC scores are smaller when the correction for the number of landmarks is applied (Tab. 2) indicating such correction is appropriate.

As expected, the geodesic and the edge set distances between the original 3D sample and the combined 2D configurations decrease as number of anatomical views increases (Tab. 2). These distances are lower when the correction is applied and become negligible when at least 4 2D sets are combined.

PLS indicates that the morphological information of the two dataset types (2D and 3D), expressed in terms of vectors of PC scores, are close to each other. In fact, the correlation coefficients are close to 1 and the *p*-values are always significant. Correlation coefficients are higher for the 2Dcomp data with the size correction than without it (Tab. 3).

The Mantel test performed between the first four PC scores of 3D data (more than 75% of the total explained variance) and those 2D data using *combinland* is equal to 0.99. The same test applied between the PC scores of 3D data and 2D combined data without "size correction" (Adams, 1999 method) returns a value equals to 0.98. We performed also the Mantel test between the 3D data and 2D combined datasets (with and without size correction) appending all the 57 possible combinations by using six 2D datasets. The results are always better if size correction is applied (i.e., *combinland*) as reported in Tab. 4.

After combining the 2D datasets we performed a Procrustes ANOVA, by using the function `procD.lm` of the `geomorph` R package, followed by pairwise comparisons of taxonomic groups (Hominoidea, Platyrrhines and Cercopithecoidea) to test for differences among groups in allometry. The shape variable consists of PC scores, the size variable (independent variable) consists on centroid sizes from 3D landmark configurations. Using 3D data or combined 2D data statistically significant differences between Cercopithecoidea-Platyrrhines and Hominoidea-Platyrrhines are always detected (Tab. 5). As shown in Fig. 11 (bottom left) the shape variations associated with the first principal component at negative and positive extreme values of the 2D and 3D data are very close to each other. Eigenvectors corresponding to the first three PCs of separate PCA are contrasted in the scatterplot matrix in Fig. 11 bottom right.

The evolutionary allometry test quantifies the relative amount of shape information (PC scores) attributable to covariation with size. The aim of this analysis is to evaluate the robustness of *combinland* method when specific analyses are performed. We found the outputs coming from 3D and 2D combined datasets close each other as reported in Tab. 5.

The distances, expressed as percentage of the maximum distance allowed, between the shapes identified by the first 20 PCs from the 3D data projected into two-dimensions and the 2D combined datasets are low, indicating high correlation between the two datasets. The average distances of the full sample expressed as percentage on each of

Table 2 – Geodesic and edge set distances calculated between the clustered tree of the 3D data and the 2D data. We considered the trees built taking into account all the specimens, the values pooled by species and the values pooled by species and gender. We reported the average values for 2D combined views. We replicated the analyses with and without the size correction.

	No size correction		With size correction	
N. of views	**Geodesic**	**Edge set**	**Geodesic**	**Edge set**
1	3.18%	103.33	3.18%	103.33
2	2.81%	91.53	2.54%	84.2
3	2.61%	83.75	2.34%	74.85
4	2.61%	79.06	2.27%	67.73
5	2.59%	75	2.22%	65.67
6	2.77%	80	2.09%	59

Table 3 – First 5 axes of covariation with percentage of the explained covariance (% cov.), coefficient of correlation (Corr.) and *p*-values calculated by performing the PLS between the PC scores coming from the 3D and 2Dcomp data with and without correction.

	No size correction			With size correction		
PLS axis	**% cov.**	**Corr.**	***p*-value**	**% cov.**	**Corr.**	***p*-value**
PLS 1	55.551	0.995	0.001	55.551	0.995	0.001
PLS 2	25.248	0.994	0.001	25.074	0.997	0.001
PLS 3	15.964	0.991	0.001	16.462	0.994	0.001
PLS 4	1.308	0.975	0.001	1.301	0.984	0.001
PLS 5	0.38	0.961	0.001	0.376	0.98	0.001

Table 4 – The Mantel test performed between the shape information encoded in 3D data and in combined 2D data with and without size correction. The average values for Z-statistic combining two, three, four, five and six 2D views are reported.

	No size correction		With size correction	
N. of views	**Z-statistic**	***p*-value**	**Z-statistic**	***p*-value**
2	0.9	0.01	0.91	0.01
3	0.93	0.01	0.95	0.01
4	0.96	0.01	0.97	0.01
5	0.97	0.01	0.98	0.01
6	0.98	0.01	0.99	0.01

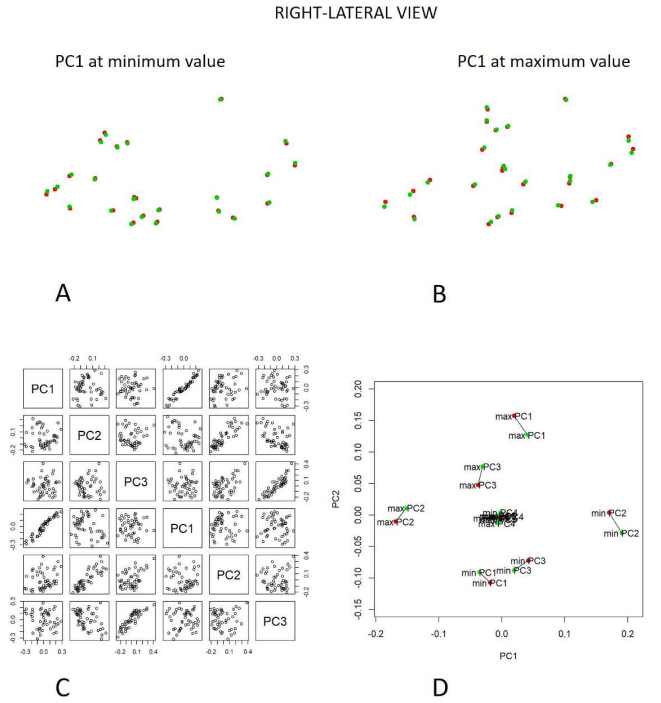

Figure 11 – Upper row: comparison of the shape variation coming from 3D and 2D datasets (right-lateral view). Plot of the Cartesian coordinates associated with the minimum and maximum values of the PCI in right-lateral view (A and B, 3D data in green and 2D data in red). Bottom left: PCA plot of the shape variations coming from 3D and 2D data (3D data in green and 2D data in red) combined together. Bottom right: scatterplot matrix performed on the eigenvectors (3D and 2D data) referred to the first three PCs (D) and coming from separate PCA.

the six anatomical views are 2.9% (anterior), 3.2% (posterior), 0.7% (superior), 5.3% (inferior), 2% (left lateral) and 2% (right lateral) (see Tab. S9 for full results).

Discussion

In landmark-based geometric morphometrics, shape variability is analysed through the definition of homologous anatomical points. Such configuration of landmarks provides the best representation of shape in the three dimensions. Nonetheless 2D data are much more common because they are easier to collect and/or less expensive, and well-suited to deal with flat biological objects, like the hemimandibles of vertebrates, the wings of insects and plants leaves (Meloro et al., 2015; Viscosi and Cardini, 2011; Klingenberg et al., 1998). Herein, we present a new R tool which allows merging shape information coming from different landmark sets. We proposed an example where different 2D views capture a 3D biological object. Adams (1999) first introduced a method to combine sets of 2D shape variables belonging to the same specimens. The relative sizes of the landmark configurations to be appended are calculated as the ratio of the two subsets *CS*. This allows to accomplish a new PCA, but the visualization of the shape variation associated to the new PC scores is somewhat complicated as a double step is needed to resort the relationship between original 2D coordinates and the PC scores of the combined analysis. Moreover, the ratio of *CS* values is not representative of the actual size differences between configurations as a specific size correction that considers the number of landmarks and dimensions is needed. The consequence of not performing such size correction is highly anecdotal as strongly dependent on the type of configurations entering the analysis and their reciprocal size differences as well as on the homogeneity of the spatial distribution of landmarks. Although this effect might be negligible under most circumstances, it might become severe when the sizes of the configurations are very different or when different sets are constituted by very different number of landmarks or when the size and shape space is used during subsets GPAs. Since the introduction of semi-landmark, in many GM studies the morphology is acquired by using semi-landmarks homogeneously distributed along curves or surfaces or on specific anatomical regions (e.g., supraorbital ridges, temporal lines, piriform aperture). The use of semi-landmark is recommended when on the anatomical structures under investigation none or a few of landmarks are detectable. Semi-landmark could be used in both 2D and 3D GM analyses. As stated in the "*Geometric morphometrics, centroid size and biological implications*" section our proposed "size correction" mitigates the problem related when different sets have a different number of landmarks. We did not use specifically semi-landmark sets in the real case presented here. However, in the simulated GM example we show exactly what could happen when combining two views composed by several landmarks as happens in semi-landmarks datasets. The performance of *combinland* is better than "traditional" method proposed by Adams (1999) when the number of landmarks of the combined configurations is different. We demonstrated that, given enough 2D information, combinland retrieves a relatively faithful representation of the morphological variation of the ordination space obtained with 3D data.

We used *combinland*, on six 2D standard anatomical views for 133 skulls belonging to 14 different primate species, obtaining 133×6=798 2D landmark configurations overall. We found that both the general reciprocal position of species in the ordination plots and variance decomposition are very similar to each other (Fig. 8– 9). Furthermore, UPGMA built on PC scores pooled by species, returned the same topological structure (edge set=0, see Tab. 6) and very low geodesic distance (1.34/100). The shape changes described by the PC scores calculated for the two sets (3D and 2D from combinland) are very close (Fig. 10). We showed that combinland replicates rather well the suite of morphological information encoded in original 3D data (Fig. 9 and Fig. S10–S14). When we asked how much 2D information is enough to gain the same insight, we found that using less than all anatomical views the results of 2D and 3D are qualitatively similar using six and four anatomical views (e.g., edge set distances from 3D results are equal to 59.00 and 67.73 respectively, for detail see Tab. 2). This is important because 2D information could not be as rich in real case studies as in our simulated one.

We therefore emphasize *combinland* could be safely used to reprocess published data coming from two or more anatomical views of the same specimens (e.g. different bony elements), or as the final processing of data coming from photo shooting, originally designed for different purposes. This could be useful when dealing with fossilised remains where the acquisition of 3D data is not easily available (e.g. the Altamura man, Lari et al., 2015), or even impossible given imperfect preservation.

In this study, we did not evaluate the influence of combining landmark data in order to face the integration and modularity between pre-

Table 5 – Procrustes ANOVA results performed on 3D and 2D combined datasets (with and without "size correction") defining the centroid size vector of 3D data as regressor. We applied the Procrustes ANOVA on three different groups: Platyrrhini, Cercopithecoidea and Hominoidea.

	3D data		Combined 2D data			
			No size correction		With size correction	
	R^2	*p*	R^2	*p*	R^2	*p*
Platyrrhini	0.459	0.001	0.437	0.001	0.434	0.001
Cercopithecoidea	0.39	0.001	0.397	0.001	0.389	0.001
Hominoidea	0.352	0.001	0.305	0.001	0.304	0.001

Table 6 – Geodesic and edge set distance calculated between UPGMA trees of the 3D data and 2D data with and without size correction. We report also the distances pooling the data by species and sex.

	Geodesic distance		Edge set distance	
Size correction	No	Yes	No	Yes
Not pooled	2.47%	2.09%	69	59
Pooled by species	1.82%	1.34%	0	0
Pooled by species and sex	2.5 %	2.19%	1	1

defined modules. For example one could use *combinland* in order to build two views for defining one module and other two views for another. Then, exploring the covariation between these modules is matter for further investigations as we did not gauge this aspect here.

Also, as stated in the Introduction, our experiment here cannot simulate the Parallax problem present in real photographs (Mallison and Wings, 2014; Mullin and Taylor, 2002) due to either lens distortion or unperfect lens positioning relatively to the specimen. In fact, by using 3D digital models the projection of landmarks on specific planes (defined by triplets of points) is eased in comparison to the real life situation of dealing with photographic devices. A further study based on the comparison between results coming 3D data analysis and those from 2D analysis performed on data extracted from real photographs should expand upon the results we presented here in order to extend our knowledge about the performance of the procedure reported in this study. Moreover, the size correction is a standardization strategy aimed at yielding a reasonable approximation for comparing sizes. Given the very nature of *CS*, comparing sizes of different shapes constituted by landmarks digitized on an external border only and on both external border and inner region could not be easy as it depends upon landmark's spatial distribution.

References

Adams D.C., 1999. Methods for shape analysis of landmark data from articulated structures. Evol. Ecol. Res. 1(8): 959–970.

Adams D.C., Otárola-Castillo E., 2013. `geomorph`: An r package for the collection and analysis of geometric morphometric shape data. Methods Ecol. Evol. 4(4): 393–399.

Adams D.C., Rohlf F.J., 2004. Slice DE. Geometric morphometrics: ten years of progress following the 'revolution.' Ital. J. Zool. 71(1): 5–16.

Adams D.C., Rohlf F.J., Slice D.E., 2013. A field comes of age: geometric morphometrics in the 21st century. Hystrix 24(1): 7–14.

Bastir M., Rosas A., 2006. Correlated variation between the lateral basicranium and the face: a geometric morphometric study in different human groups. Arch. Oral. Biol. 51(9): 814–824.

Bastir M., Rosas A., 2009. Mosaic evolution of the basicranium in *Homo* and its relation to modular development. Evol. Biol. 36(1): 57–70.

Bates K.T., Falkingham P.L., Rarity F., Hodgetts D., Purslow T., Manning P.L., 2010. Application of high-resolution laser scanning and photogrammetric techniques to data acquisition, analysis and interpretation in palaeontology. Int. Arch. Photogramm. Remote Sens. Spat. Inf. Sci. 38(5): 68–73.

Blumenbach J.F., Bendyshe T., Marx K., Flourens P., Wagner R., Hunter J., 1865. The Anthropological Treatises of Johann Friedrich Blumenbach. Anthropological Society.

Bookstein F.L., 1986. Size and shape spaces for landmark data in two dimensions. Stat. Sci. 1(2): 181–222.

Bookstein F.L., 1989. Size and shape: A comment on semantics. Syst. Biol. 38(2): 173–180.

Cardini A., 2014. Missing the third dimension in geometric morphometrics: how to assess if 2D images really are a good proxy for 3D structures? Hystrix 25(2): 73–81.

Chakerian J., Holmes S., 2012. Computational tools for evaluating phylogenetic and hierarchical clustering trees. J. Comput. Graph. Stat. 21(3): 581–599.

Cunningham J.A., Rahman I.A., Lautenschlager S., Rayfield E.J., Donoghue P.C.J., 2014. A virtual world of paleontology. Trends Ecol. Evol. 29(6): 347–357.

Davies T.G., Rahman I.A., Lautenschlager S., Cunningham J.A., Asher R.J., Barrett P.M., Bates K.T., Bengtson S., Benson R.B.J., Boyer D.M., Braga J., Bright J.A., Claessens L.P.A.M., Cox P.G., Dong X.P., Evans A.R., Falkingham P.L., Friedman M., Garwood R.J., Goswami A., Hutchinson J.R., Jeffery N.S., Johanson Z., Lebrun R., Martínez-Pérez C., Marugán-Lobón J., O'Higgins P.M., Metscher B., Orliac M., Rowe T.B., Rücklin M., Sánchez-Villagra M.R., Shubin N.H., Smith S.Y., Starck J.M., Stringer C., Summers A.P., Sutton M.D., Walsh S.A., Weisbecker V., Witmer L.M., Wroe S., Yin Z., Rayfield E.J., Donoghue P.C.J., 2017. Open data and digital morphology. Proc. R. Soc. B Biol. Sci. 284(1852): 20170194.

Davis M.A., Douglas M.R., Collyer M.L., Douglas M.E., 2016. Deconstructing a species-complex: Geometric morphometric and molecular analyses define species in the Western Rattlesnake (*Crotalus viridis*). PLoS ONE 11(1): e0146166.

DeQuardo J.R., Keshavan M.S., Bookstein F.L., Bagwell W.W., Green W.D.K., Sweeney J.A., Haas G.L., Tandon R., Schooler N.R., Pettegrew J.W., 1999. Landmark-based morphometric analysis of first-episode schizophrenia. Biol. Psychiatry 45(10): 1321–1328.

Dryden I.L., Mardia K.V., 2016. Statistical shape analysis, with applications in R: Second edition.

Gower J.C., 1975. Generalized procrustes analysis. Psychometrika 40(1): 33–51.

Jungers W.L., Falsetti A.B., Wall C.E., 1995. Shape, relative size, and size-adjustments in morphometrics. Am. J. Phys. Anthropol. 38(S21): 137–161.

Kendall D.G., 1977. The diffusion of shape. Adv. Appl. Probab. 9(3): 428–430.

Klingenberg C.P., 2013. Visualizations in geometric morphometrics: how to read and how to make graphs showing shape changes. Hystrix, Ital. J. Mammal. 24(1): 15–24.

Klingenberg C.P., McIntyre G.S., Zaklan S.D., 1998. Left-right asymmetry of fly wings and the evolution of body axes. Proc. R. Soc. B Biol. Sci. 265(1402): 1255–1259.

Lari M., Di Vincenzo F., Borsato A., Ghirotto S., Micheli M., Balsamo C., Collina C., De Bellis G., Frisia S., Giacobini G., Gigli E., Hellstrom J.C., Lannino A., Modi A., Pietrelli A., Pilli E., Profico A., Ramirez O., Rizzi E., Vai S., Venturo D., Piperno M., Lalueza-Fox C., Barbujani G., Caramelli D., Manzi G., 2015. The Neanderthal in the karst: first dating, morphometric, and paleogenetic data on the fossil skeleton from Altamura (Italy). J. Hum. Evol. 82(1): 88–94. doi:10.1016/j.jhevol.2015.02.007

Mallison H., Wings O., 2014. Photogrammetry in paleontology–a practical guide. J. Paleontol. Tech.

Meloro C., Cáceres N.C., Carotenuto F., Sponchiado J., Melo G.L., Passaro F., Raia P., 2015. Chewing on the trees: Constraints and adaptation in the evolution of the primate mandible. Evolution 69(7): 1690–1700.

Meloro C., Hunter J., Tomsett L., Portela Miguez R., Prevosti F.J., Brown R.P., 2017. Evolutionary ecomorphology of the Falkland Islands wolf *Dusicyon australis*. Mamm. Rev. 47(2): 159–163.

Mullin S.K., Taylor P.J., 2002. The effects of parallax on geometric morphometric data. Comput. Biol. Med. 32(6): 455–464.

Neaux D., Sansalone G., Ledogar J.A., Ledogar S.H., Luk T.H.Y., Wroe S., 2018. Basicranium and face: Assessing the impact of morphological integration on primate evolution. J. Hum. Evol. 118: 43–55.

Olsen A.M., Westneat M.W., 2015. StereoMorph: An R package for the collection of 3D landmarks and curves using a stereo camera set-up. Methods Ecol. Evol. 6(3): 351–356.

Owen M., Provan J.S., 2011. A fast algorithm for computing geodesic distances in tree space. IEEE/ACM Trans. Comput. Biol. Bioinforma. 8(1): 2–13.

Piras P., Buscalioni A.D., Teresi L., Raia P., Sansalone G., Kotsakis T., Cubo J., 2014. Morphological integration and functional modularity in the crocodilian skull. Integr. Zool. 9(4): 498–516.

Piras P., Marcolini F., Raia P., Curcio M., Kotsakis T., 2010. Ecophenotypic variation and phylogenetic inheritance in first lower molar shape of extant Italian populations of *Microtus (Terricola) savii* (Rodentia). Biol. J. Linn. Soc. 99(3): 632–647.

Piras P., Teresi L., Buscalioni A.D., Cubo J., 2009. The shadow of forgotten ancestors differently constrains the fate of Alligatoroidea and Crocodyloidea. Glob. Ecol. Biogeogr. 18(1): 30–40.

Piras P., Teresi L., Traversetti L., Varano V., Gabriele S., Kotsakis T., Raia P., Puddu P.E., Scalici M., 2016. The conceptual framework of ontogenetic trajectories: Parallel Transport allows the recognition and visualization of pure deformation patterns. Evol. Dev. 18(3): 182–200.

Ponton D., 2006. Is geometric morphometrics efficient for comparing otolith shape of different fish species? J. Morphol. 267(6): 750–757.

Profico A., Bellucci L., Buzi C., Di Vincenzo F., Micarelli I., Strani F., Tafuri M.A., Manzi G., 2018a. Virtual anthropology and its application in cultural heritage studies. Stud. Conserv. 64(6): 1–14.

Profico A., Schlager S., Valoriani V., Buzi C., Melchionna M., Veneziano A., Raia P., Moggi-Cecchi J., Manzi G., 2018b. Reproducing the internal and external anatomy of fossil bones: two new automatic digital tools. Am. J. Phys. Anthropol. 166(4): 979-986.

Profico A., Veneziano A., Buzi C., Melchionna M., Raia P., 2019. Geometric Morphometrics Analyses. https://github.com/Arothron.

Rohlf F.J., 2000. On the use of shape spaces to compare morphometric methods. Hystrix 11(1): 9–25.

Rohlf F.J., Corti M., 2000. Use of two-block partial least-squares to study covariation in shape. Syst. Biol. 49(4): 740–753.

Rohlf F.J., Marcus L.F., 1993. A revolution morphometrics. Trends Ecol. Evol. 8(4): 129–132.

Sansalone G., Kotsakis T., Piras P., 2015. *Talpa fossilis* or *Talpa europaea*? Using geometric morphometrics and allometric trajectories of humeral moles remains from Hungary to answer a taxonomic debate. Palaeontol. Electron. 18(2): 1–17.

Sokal R.R., Michener C., 1958. A statistical method for evaluating systematic relationships.

Varano V., Gabriele S., Teresi L., Dryden I.L., Puddu P.E., Torromeo C., Piras P., 2017. The TPS Direct Transport: A New Method for Transporting Deformations in the Size-and-Shape Space. Int. J. Comput. Vis. 124(3): 384–408.

Varano V., Piras P., Gabriele S., Teresi L., Nardinocchi P., Dryden I.L., Torromeo C., Puddu P.E., 2018. The decomposition of deformation: New metrics to enhance shape analysis in medical imaging. Med. Image Anal. 46: 35–56.

Veneziano A., Landi F., Profico A., 2018. Surface smoothing, decimation, and their effects on 3D biological specimens. Am. J. Phys. Anthropol. 166(2): 473–480.

Viscosi V., Cardini A., 2011. Leaf morphology, taxonomy and geometric morphometrics: A simplified protocol for beginners. PLoS ONE 6(10): e25630.

Weber G.W., 2005. Virtual anthropology. Am. J. Phys. Anthropol. 156(S59): 22–42.

Associate Editor: P. Colangelo

Supplemental information

Additional Supplemental Information may be found in the online version of this article:

Figure S1 3D landmark configuration shown on a specimen of *Macaca arctoides*.

Table S2 List of the samples used.

Figure S3 The six 2D landmark configurations showed on a specimen of *M. arctoides*.

Table S4 List of the landmark used.

Figure S5 Cluster analysis of the shape in the simulated case study.

Figure S6 Plot of the first two PCs of the 3D and 2D data pooled by species.

Figure S7 Cluster analysis of the PCs pooled by species and gender of the 3D and 2D data.

Figure S8 Plot of the first two Principal Components for the 2D (left) and 3D (right) data.

Table S9 Procrustes distances, expressed as percentage of the maximum distance allowed, between 2D data and 3D data.

Figure S10 Comparison of the shape variation coming from 3D and 2D datasets along the anterior view.

Figure S11 Comparison of the shape variation coming from 3D and 2D datasets along the posterior view.

Figure S12 Comparison of the shape variation coming from 3D and 2D datasets along the superior view.

Figure S13 Comparison of the shape variation coming from 3D and 2D datasets along the inferior view.

Figure S14 Comparison of the shape variation coming from 3D and 2D datasets along the left-lateral vie.